nature communications

Article

https://doi.org/10.1038/s41467-025-60416-x

A biomimetic multi-component subunit vaccine via ratiometric loading of hierarchical hydrogels

Received: 10 April 2024

Accepted: 22 May 2025

Published online: 01 July 2025

Check for updates

Fanfan Du[1,2,6], Simseok A. Yuk[2,6], Yuan Qian[2,6], El Hadji Arona Mbaye[2], Michael P. Vincent[2], Sharan Bobbala[2], Tirzah M. Abbott[3], Hyeohn Kim[2], Yang Li[4], Haoyu Li[2], Sijia Yi[2], Baofu Qiao[5] & Evan A. Scott[1,2]

The development of subunit vaccines that mimic the molecular complexity of attenuated vaccines has been limited by the difficulty of intracellular co-delivery of multiple chemically diverse payloads at controllable concentrations. We report on hierarchical hydrogel depots employing simple poly(-propylene sulfone) homopolymers to enable ratiometric loading of a protein antigen and four physicochemically distinct adjuvants in a hierarchical manner. The optimized vaccine consisted of immunostimulants either adsorbed to or encapsulated within nanogels, which were capable of noncovalent anchoring to subcutaneous tissues. In female BALB/c and C57BL/6 mice, these 5-component nanogel vaccines demonstrated enhanced humoral and cell-mediated immune responses compared to formulations with standard single adjuvant and antigen pairing. The use of a single simple homopolymer capable of rapid and stable loading and intracellular delivery of diverse molecular cargoes holds promise for facile development and optimization of scalable subunit vaccines and complex therapeutic formulations for a wide range of biomedical applications.

Effective vaccination relies on the ability to induce humoral and cellular immunity, with the nature of this adaptive immune response being highly dependent on the co-delivery of distinct antigen and adjuvant combinations to innate immune cells. Mimicking the diverse spectrum of immunostimulation elicited by attenuated viral and bacterial vaccines has remained a challenge for subunit vaccine formulations, which typically pair a single adjuvant and antigen for simplicity and scalability[1–3]. Furthermore, despite recent advances in creating hydrogels capable of sustained delivery of protein antigens[4–6], approaches to combine antigens with physicochemically distinct adjuvants remain challenging. In particular for hydrophobic and charged macromolecular adjuvants in the form of lipids, small molecules, or nucleic acids, controlling the concentration and stability of each during multi-component loading within a hydrophilic network is rarely achieved[7]. To this end, nanocomposite and micelle-cross-linked hydrogels[8,9] have been used to load hydrophobic cargoes[10]. These hierarchical materials are assembled via multi-length scale processes and frequently possess biomimetic properties that include multi-functionality, environmental responsiveness, and self-organization[11]. The fabricating process for the artificial hierarchical structures is, however, tedious and the applied synthetic components are complex.

Here, we report on hierarchical hydrogels, assembled from a single simple homopolymer via a multi-stage process, that enable ratiometric loading and delivery of four physicochemically distinct adjuvants along with a protein-based antigen (Fig. 1). Starting with a poly(propylene sulfone) (PPSU)[12] solution, the addition of water

[1]Department of Biomedical Engineering, NanoSTAR Institute, University of Virginia School of Medicine, Charlottesville, VA, USA. [2]Department of Biomedical Engineering, Northwestern University, Evanston, IL, USA. [3]Northwestern University Atomic and Nanoscale Characterization Experimental Center, Evanston, IL, USA. [4]Department of Chemical and Biological Engineering, Northwestern University, Evanston, IL, USA. [5]Department of Natural Sciences, Baruch College, City University of New York, New York, NY, USA. [6]These authors contributed equally: Fanfan Du, Simseok A. Yuk, Yuan Qian. e-mail: evan.scott@virginia.edu

https://doi.org/10.1038/s41467-025-60416-x

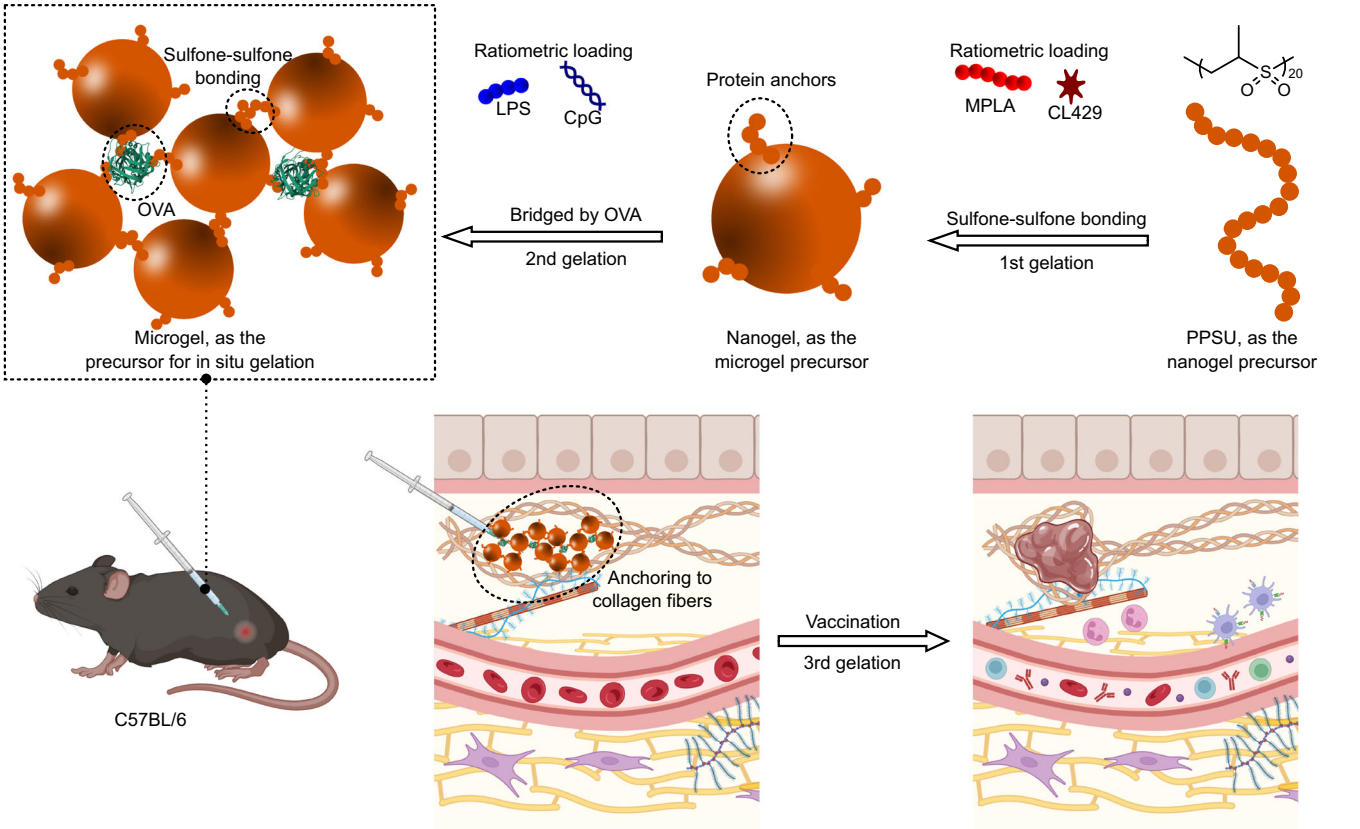

Fig. 1 | Schematic of PPSU-based hierarchical hydrogels that enable ratiometric loading of multiple adjuvants for vaccine optimization. Hydrophobic adjuvants are encapsulated through network assembly of PPSU (1st gelation). Water-soluble adjuvants are adsorbed during the formation of microgels triggered by bridging nanogels with the antigen OVA (2nd gelation, only simple mixing steps that take less than 5 min before injection). Microgels anchor onto collagens upon subcutaneous injection (3rd gelation), allowing sustained release. Within the first 24 h after vaccination, Th1/Th2 cytokine levels increased. By day 7, anti-OVA IgM antibodies had risen, and over the subsequent four days, the vaccination effectively promoted the proliferation of adoptively transferred antigen-specific T cells. Anti-OVA IgG2b and IgG2c responses remained significantly elevated for up to one month, while significant levels of anti-OVA IgG1 antibodies persisted through day 84. Following a prime-boost administration on day 90 and a subsequent 15-day period, marked increases in neutrophils, $CD11b^+$ conventional dendritic cells (cDCs), and B cells were observed.

promotes interchain sulfone-sulfone bonding, yielding nanogels with short PPSU coronas capable of self-bonding or protein anchoring. When transferred into protein solutions in saline, the nanogels irreversibly aggregate into microgels as a secondary structure via surface fusion or protein bridging. Following subcutaneous injection, the microgels then bind to extracellular matrix components, mainly collagen fibers, via PPSU coronas to form stable in situ nanocomposite hydrogels as the tertiary structure. The delivery system takes advantage of efficient loading (>90%) throughout the process, allowing us to develop an optimized vaccine formulation that consists of monophosphoryl lipid A (MPLA)[13], CL429[14], CpG oligodeoxynucleotides (ODN)[15], lipopolysaccharide (LPS)[16], and the protein antigen ovalbumin (OVA). In vitro and in vivo experiments demonstrate enhanced humoral and cell-mediated immune responses for these five-component nanogel vaccines compared to formulation with a more standard single adjuvant and antigen pair.

Results and discussion

Ratiometric loading of five separate vaccine immunostimulants

The preparation of PPSU nanogels has been described in our previous publications[12,17]. As prepared, the nanogels have a zeta potential between −30 and −40 mV[12,17] that prevents aggregation in water. Importantly, the coronas of the nanogels consist of "living" PPSU that will undergo further sulfone-sulfone bonding on demand. This PPSU corona is also capable of anchoring proteins while preserving protein bioactivities at the interfaces[17]. We investigated nanogel aggregation in aqueous solutions, a requirement to inhibit cell uptake through the formation of microgels before subcutaneous injection (Supplementary Fig. S1). The strategy involves the addition of salts to promote corona fusion by shielding the electrostatic repulsion among nanogels, or the use of low concentration protein solutions (e.g. hemoglobin, neutral charged) in water to bridge two nanogels through surface adsorption. By employing protein payloads as the crosslinking agent, the minimalist secondary microgels engineered here do not require additional cross-linking agents or stabilizers, allowing rapid and simple preparation of a protein-based microgel suspension that is amenable to facile injection.

We explored the versatility and universality of this system by extending the study to other proteins, such as OVA. Although PPSU surfaces show high affinity to nonspecific proteins, the formation of OVA-based microgels was achieved in phosphate buffered saline (PBS) rather than in water (Fig. 2a) because the presence of salts is required to trigger the adsorption of highly negatively charged proteins[17]. That is, incubating PPSU nanogels in PBS with OVA leads to hybrid microgels through both corona fusion and crosslinking via protein antigen bridges (Fig. 2b, c and Supplementary Fig. S2). The microgels are not only bioactive based on the demonstrated protein adsorption mechanism[17], but also support the pre-encapsulation of physicochemically distinct adjuvants given their high encapsulation efficiencies (>95%) for a wide range of organic cargoes[12].

Amphiphiles can also to be loaded during the formation of microgels. We demonstrated, both experimentally and through

https://doi.org/10.1038/s41467-025-60416-x

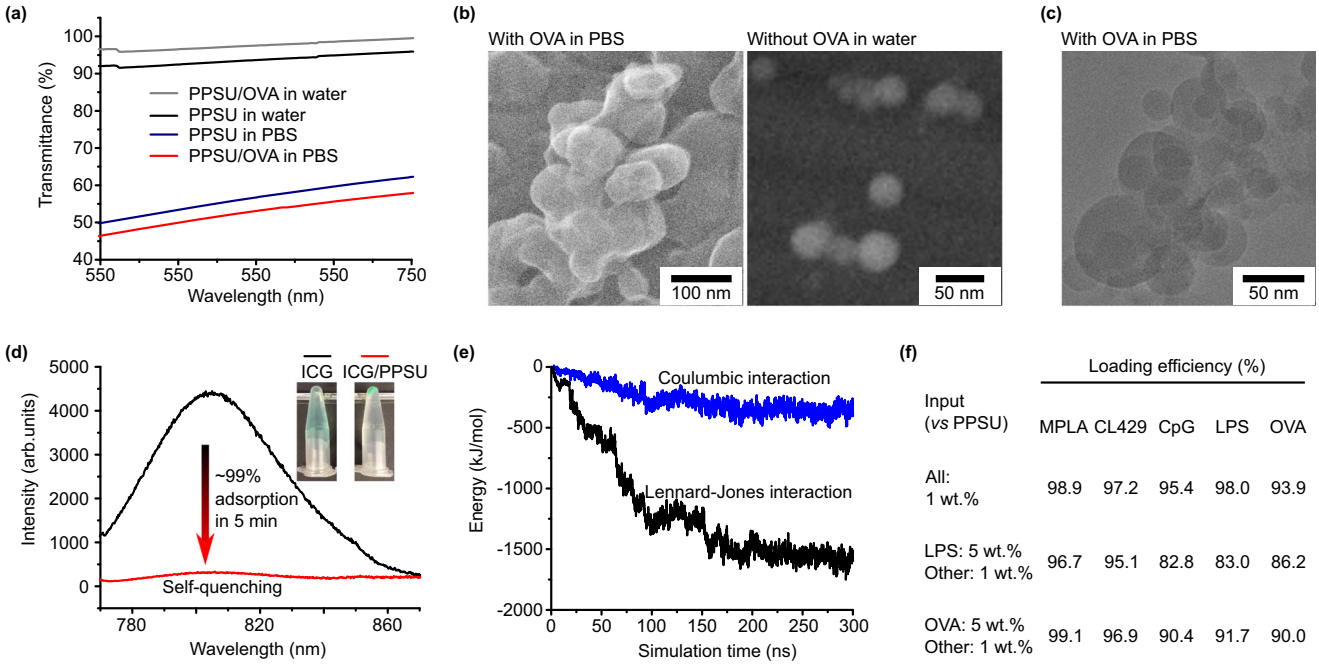

Fig. 2 | PPSU nanogels enable the ratiometric loading of multiple cargoes and subsequent assembly into microgels. a Comparison of the extinction spectra of the mixture of PPSU nanogels (1 mg/mL) with 1 wt.% of OVA in PBS or water. **b** CryoSEM of PPSU microgels following salt-induced gelation of nanogels via OVA bridges in PBS. **c** CryoTEM of PPSU microgels formed by mixing PPSU nanogels with OVA in PBS. (b-c) All experiments were independently repeated three times. **d** The complete self-quenching indicates the efficient capture of ICG during the formation of microgels in PBS. The inset shows ICG/PBS solutions before and after the addition of PPSU nanogels. The photos were taken after centrifugation. **e** Computational studies suggest that the PPSU surface is capable of molecular capture through hydrophobic interactions (Lennard-Jones). **f** Multiple adjuvants, including MPLA, CL420, CpG, and LPS can be co-loaded in a ratiometric manner while using the antigen OVA to bridge nanogels.

simulations, the preserved affinity of PPSU surfaces to capture amphiphilic cargoes in aqueous solution during microgel formation. When we mixed PPSU nanogels with indocyanine green (ICG) in PBS, we detected by fluorescence measurements the efficient (~99%) and rapid (<5 min) adsorption of the dye, which completely quenched the fluorescence (Fig. 2d). Near 100% adsorption of many other amphiphilic dyes at PPSU interfaces were shown in our previous report[17]. Explicit solvent all-atom molecular dynamics simulations were performed for mixtures of 10 ICG molecules and a PPSU nanogel in water, showing that all ICG molecules were adsorbed by the nanogel (Fig. 2e and Supplementary Fig. S3). The simulation revealed that the adsorption is directed by hydrophobic interactions, consistent with our previous findings for the adsorption of proteins[17]. These results essentially suggest that efficient adsorption can be generalized to diverse therapeutics and biologics that have amphiphilic properties.

We explored the versatility and universality of PPSU by optimizing the loading of diverse adjuvants. Vesicular nanostructures (e.g. liposomes and polymersomes) typically display low encapsulation efficiency for water-soluble cargoes[18–20]. Micelles show efficient loading only for hydrophobic molecules[21], whereas conventional hydrogels can only trap hydrophilic solutes[6]. By contrast, PPSU hydrogels showed > 90% loading efficiencies for all these mentioned types of cargoes (Supplementary Fig. S4), including MPLA (non-ionic lipid amphiphile), CL429 (hydrophobic small molecule), CpG (hydrophilic nucleic acid), LPS (ionic lipid amphiphile), and OVA (protein). Because vaccine responses can be modulated and customized via the simultaneous delivery of multiple synergistic adjuvants[22], we further demonstrated the ability of PPSU hydrogels to effectively co-load the antigen with all four adjuvants, showing that the resulting formulations can be easily controlled by the input ratios (Fig. 2f). Of note, these formulations mimic the full range of immunostimulation of an attenuated bacterium[23–25].

In situ formation of PPSU tertiary hydrogels upon administration

Because the surfaces of the microgels were not exposed to excess protein for passivation[17], we hypothesized that surface-accessible domains would be available for subsequent tissue attachment upon subcutaneous injection. This was confirmed by a model experiment in which we dropped the suspension of PPSU microgels onto an excised skin and observed an immediate immobilization of the microgels (Fig. 3a and Supplementary Fig. S5). We then subcutaneously injected PPSU microgels and extracted the in situ formed tertiary hydrogels 30 min after administration. Frequency-dependent oscillatory experiments conducted in a linear viscoelastic regime revealed that the gels exhibited a storage modulus comparable to the local biological tissues (Fig. 3b)[26,27]. The consistently higher maintenance of the storage modulus (G′) over the loss modulus (G″) across the evaluated frequency range indicated the solid-like properties necessary for robust hydrogel formation, thereby confirming a process of in situ gelation upon subcutaneous administration (Fig. 3c).

We tracked by scanning electron microscopy (SEM) imaging the in situ gelation of PPSU microgels within tissues after the injection (Fig. 3d and Supplementary Fig. S6). The results showed that the microgels adhered to the surface of collagen fibers 30 min post administration. Adhesion of the microgels towards the collagen fibers was also verified at day 5 post injection (Fig. 3d). Fusion between PPSU and other surrounding tissues was also found (Supplementary Fig. S7). The process of in situ gelation was accompanied by a decrease in the gel volume (Supplementary Fig. S8). As a further demonstration, we loaded the microgels with Fe^{3+} for energy-dispersive X-ray spectroscopy (EDS) elemental mapping (Supplementary Fig. S9) and confirmed SEM-EDS colocalization of Fe^{3+} that differentiated the tertiary PPSU hydrogels from collagen fibers (Fig. 3e).

https://doi.org/10.1038/s41467-025-60416-x

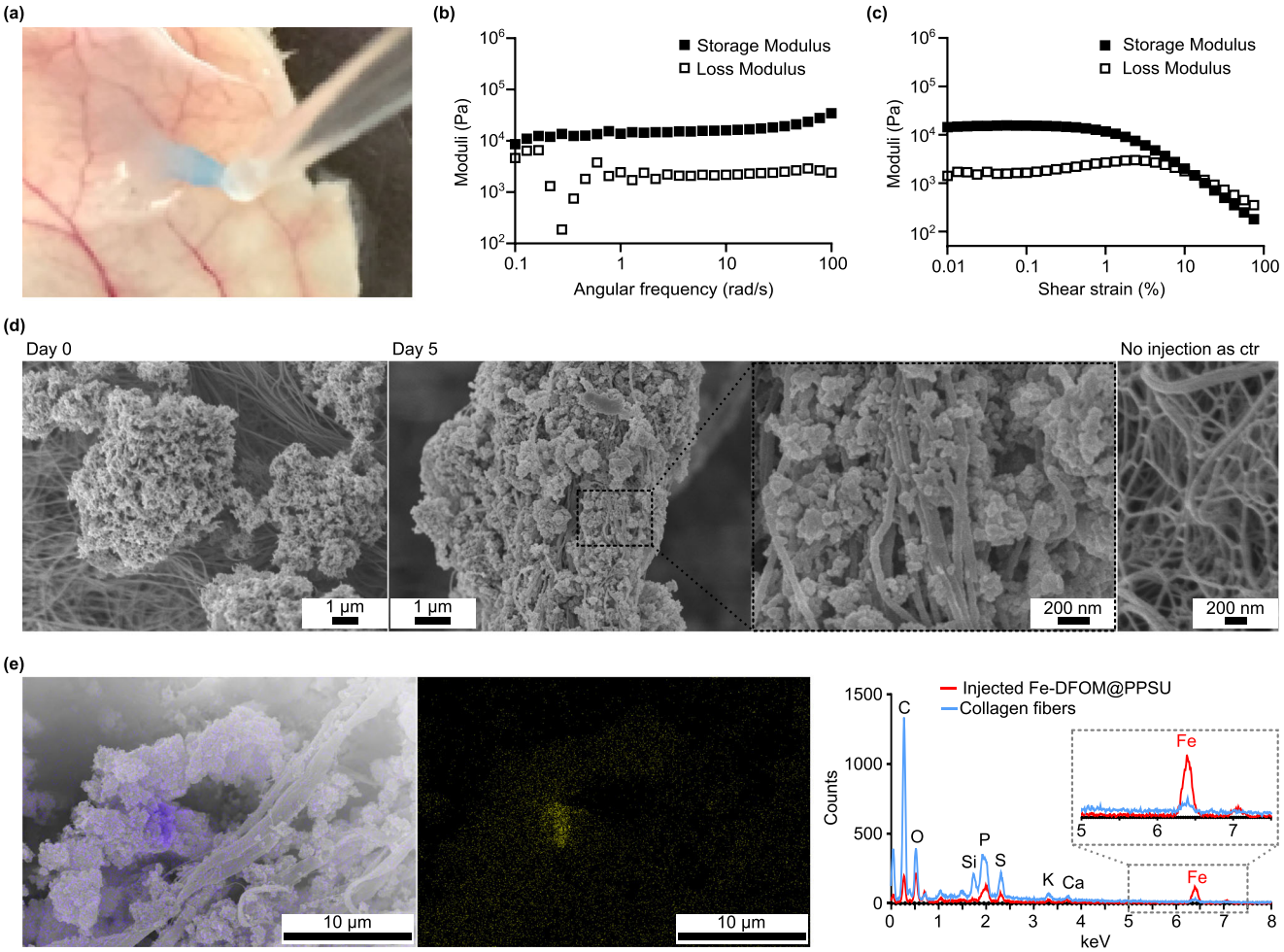

Fig. 3 | Characterization of tissue-bound hydrogels that formed following subcutaneous injection of PPSU microgels. a Dropping PPSU microgels (colored by ICG) onto an excised skin mimics the process of subcutaneous injection, anchoring the microgels onto tissues. **b** Frequency-dependent oscillatory experiments conducted in a linear viscoelastic regime. **c** The storage and loss moduli across the evaluated frequency range. (b-c) Rheological measurements were performed on excised samples 30 min post injection, demonstrating the in-situ formation of tertiary hydrogels. **d** SEM images of excised gels on day 0 (30 min post injection) and 5 days post injection. The SEM image of collagen fibers is included for comparison (ctr = control). **e** EDS elemental mapping of Fe^{3+}-loaded hydrogels 30 min post injection. **d**, **e** All experiments were independently repeated three times.

Having obtained evidence that the tertiary hydrogels form upon subcutaneous injection, we investigated the reversibility of the hierarchical structure and ruled out the possibility of releasing nanogels from the tertiary hydrogels (Supplementary Fig. S10). We then employed the tertiary hydrogels as depots for the sustained release of diverse cargoes. Real-time whole-body imaging showed that the administration of ICG-adsorbed microgels achieved prolonged release of ICG (Fig. 4a and Supplementary Fig. S11). Given the possibility that encapsulated cargoes could have slower release rates than their adsorbed counterparts, we proceeded to investigate the effect of our drug loading strategy on in vivo release kinetics. Förster resonance energy transfer (FRET)[28] was applied as a tool in the comparison study to exclude the interference of concentration-induced fluorescence quenching. FRET imaging of the excised skins was used to monitor the in vivo release of a FRET pair consisting of encapsulated Rhodamine 6 G (Rh6G) and adsorbed Rh101. With the fluorescence of the encapsulated Rh6G nearly completely quenched by the adsorption of Rh101 (Fig. 4b and Supplementary Fig. S12), a burst release of Rh101 at 1 day post injection was revealed by the recovery of Rh6G fluorescence (Fig. 4c). Sustained release of the two dyes began on day 3, achieved through the liquefication of the tertiary hydrogels. These results demonstrated an erosion-controlled release process for the encapsulated dyes, whereas the release of the adsorbed dyes could be first triggered by protein replacement, a diffusion-controlled process that depends on the accessibility of nanogel surfaces. Not all the nanogel surfaces are accessible to proteins during the formation of the secondary hydrogels in PBS. This was confirmed by the inefficient FRET shown in Fig. 4d, where the adsorption of excess TNF-α only partially decreased the fluorescence intensity of the encapsulated MFT. The subsequent in vivo release demonstrated an erosion-controlled release process of up to 92 days for both the cargoes (Fig. 4e and Supplementary Fig. S13), regardless of the loading strategies. Note that the release of the adsorbed TNF-α was slower than that of the adsorbed Rh101 (Supplementary Fig. S14), likely due to the increased hydrophobic interactions between PPSU nanogels and higher molecular weight proteins relative to small molecule dyes.

Employing PPSU hydrogels for multi-component vaccine optimization

The sustained release system investigated here takes advantage of three levels of physical binding (sulfone binding, then protein adsorption, and ultimately tissue binding), leading to hierarchical architectures from a simple homopolymer structure. It would allow us to design multi-component vaccines that typically require a tedious or impractical process for optimizing the concentration and ratio for each adjuvant. To this end, we used RAW-blue macrophages to assess

https://doi.org/10.1038/s41467-025-60416-x

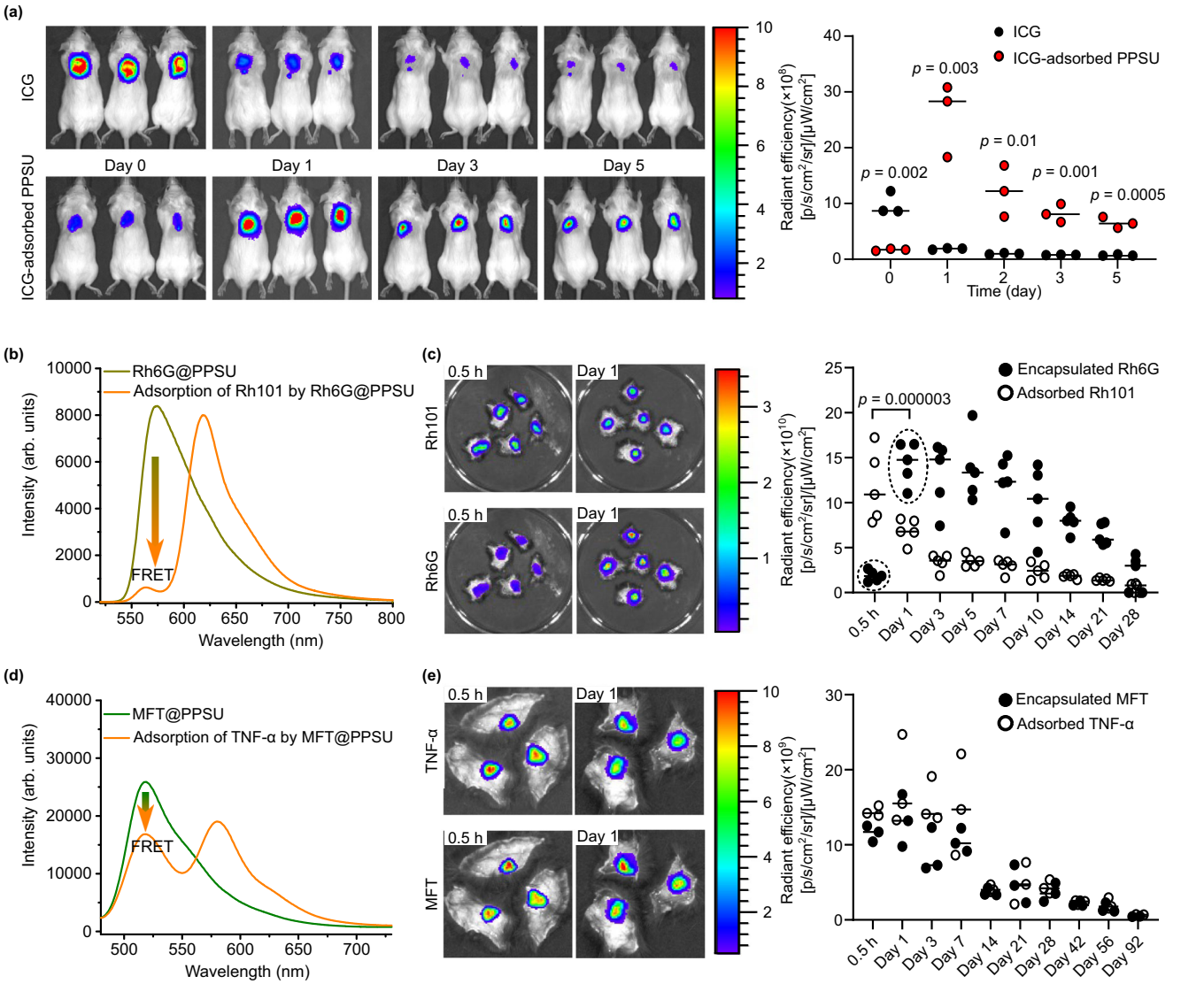

Fig. 4 | In vivo release of model cargoes loaded within PPSU microgels. a Real-time whole-body imaging of adsorbed ICG after SC injection showed prolonged release of hydrogel cargo. The data are presented as mean values with the statistical significance determined by a two-sample *t*-test ($n = 3$ mice per group). **b** Efficient FRET demonstrates full accessibility (within ~10 nm) of the microgel surfaces by small molecule fluorophore Rh101. **c** The recovery of Rh6G fluorescence at day 1 indicated quick desorption/replacement of adsorbed Rh101 upon SC injection. $\lambda_{em}/\lambda_{ex} = 465/640$ nm for Rh101, $\lambda_{em}/\lambda_{ex} = 465/560$ nm for Rh6G. The data are presented as mean values with the statistical significance determined by a two-sample *t*-test ($n = 5$ mice per group). **d** Not all of the microgel surfaces are accessible to proteins, as suggested by the inefficient FRET from encapsulated MFT in response to incubation with TNF-α. **e** Sustained release was achieved for the encapsulated MFT and adsorbed proteins. $\lambda_{em}/\lambda_{ex} = 465/600$ nm for TNF-α, $\lambda_{em}/\lambda_{ex} = 465/520$ nm for MFT. The data are presented as mean values with $n = 3$ mice per group.

retention of adjuvant bioactivity upon loading by PPSU at a low, mild, and high concentration, based on their published effective ranges (Supplementary Fig. S15)[29–33]. The results showed that PPSU alone had no effect on RAW-blue macrophages, whereas the adjuvant-loaded nanogels (microgel precursors) induced the activation of NF-kB. They have either equally effective or even enhanced activities compared to the free form adjuvants of LPS and CL429, respectively.

To determine the immunogenicity of the 5-component formulation (OVA-bridged PPSU microgels with four adjuvants, termed PPSU-4Ad) on antigen-presenting cells (APCs), PPSU-4Ad, CpG-loaded PPSU (PPSU-CpG), and OVA-loaded PPSU (PPSU-OVA) were incubated with primary C57BL/6 bone marrow-derived dendritic cells (BMDCs). Of note, for all OVA-based immunizations, each formulation contained an identical amount of OVA antigen. After 24 h, activation marker expression of the BMDCs, including MHC-II, CD40, CD80, and CD86, were assessed by flow cytometry. Low immunogenicity for PPSU-OVA was confirmed, as indicated by the same level of expression for all tested markers as that of the PBS group. But PPSU-4Ad strongly activated CD40, CD80 and CD86 expression on BMDCs, whereas the single adjuvant-loaded group (PPSU-CpG) only marginally activated CD40 and CD86 (Supplementary Fig. S16). Moreover, PPSU-4Ad stimulated MHC-II expression. These results verify that simultaneous delivery of antigen and adjuvants by PPSU-4Ad to APCs can induce a strong immunostimulatory response.

C57BL/6 mice were then immunized subcutaneously with either PPSU-CpG or PPSU-4Ad (Fig. 5a, LPS was not included as an adjuvant for cytokine and antibody experiments). Blank PPSU and PBS groups were included as controls. At 24 h post-injection, PPSU-4Ad induced both Th1 and Th2 serum cytokines (Fig. 5b). The elevated Th2 cytokine levels indicate a tendency for PPSU-4Ad to favor humoral responses[34]. Seven days post-immunization, mice immunized with PPSU-4Ad showed a significant increase in anti-OVA IgM antibodies compared to those immunized with PPSU-CpG or the blank PPSU and PBS controls (Fig. 5c). Additionally, C57BL/6 mice were subcutaneously

https://doi.org/10.1038/s41467-025-60416-x

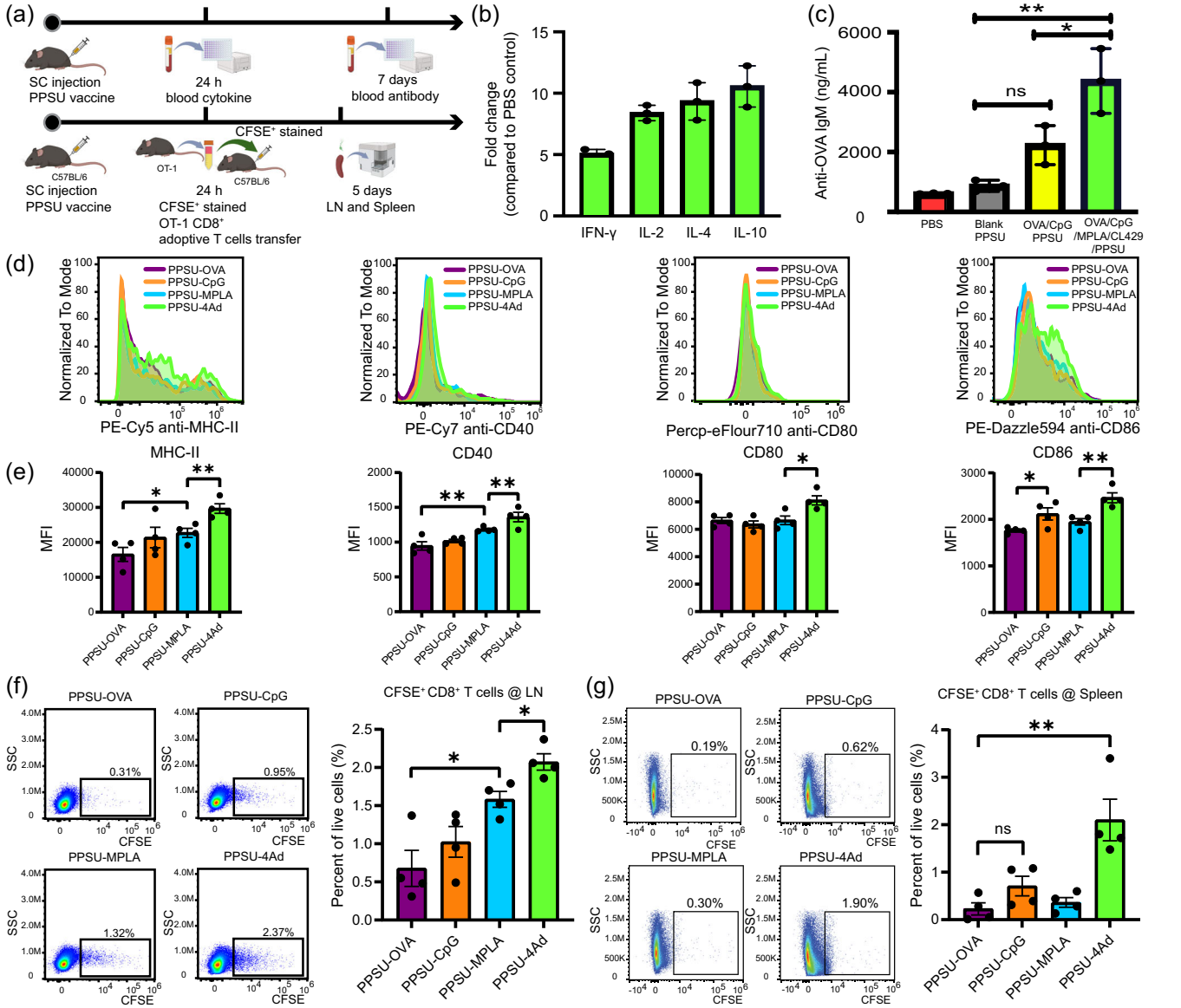

Fig. 5 | Validation of multi-adjuvant/antigen-loaded PPSU hydrogels as a subunit vaccine. a Schematic schedule of in vivo blood analysis and adoptive T cell transfer. (created with BioRender.com). **b** Cytokine fold changes 24 h after subcutaneous injection of the multi-antigen/adjuvant (LPS excluded) loaded PPSU relative to PBS control in mice. $n = 3$ mice per group (mean ± s.d). **c** Blood anti-OVA IgM antibody levels 7 days post subcutaneous administration of the multi-antigen/adjuvant (LPS excluded) loaded PPSU relative to single adjuvant, blank PPSU and PBS controls. $n = 3$ mice per group (mean ± s.d), with $^{*}p$ (0.0355) < 0.05, $^{**}p$ (0.0034) < 0.01, determined using one-way ANOVA followed by Tukey's multiple comparison test. **d** Flow cytometry histogram and **e** mean fluorescence intensity (MFI) of activation markers (MHC-II, CD40, CD80, and CD86) on dendritic cells in the lymph node after 4 days following the adoptive transfer of carboxyfluorescein succinimidyl ester (CFSE) stained $CD8^+$ T cell from OT-1 mice to C57BL/6 mice. $n = 4$ mice per group (mean ± s.d). $^{*}p$ (0.0411, MHC-II), p (0.044, CD40), p (0.0193, CD80), p (0.0393, CD86) < 0.05, $^{**}p$ (0.0099, MHC-II), p (0.0092, CD40), p (0.0067, CD86) < 0.01, and ns: not significant by unpaired two-tailed t-test. **f** Gating strategies and percentage of live $CFSE^+CD8^+$ T cells at lymph node. $n = 4$ mice per group (mean ± s.d). $^{*}p$ (0.0127, and 0.0169) < 0.05 by unpaired two-tailed t-test. and **g** spleen after 4 days post adoptive T cell transfer. $n = 4$ mice per group (mean ± s.d). $^{**}p$ (0.0064) < 0.01, and ns not significant by unpaired two-tailed t-test.

injected with either PPSU-LPS or PPSU-4Ad. The hydrogels were retrieved 30 min post-injection and incubated in transwell inserts with RAW-Blue macrophages to assess the sustained release of adjuvants. NF-κB/AP-1 activation remained lower for both hydrogels compared to nanogels and bolus formulations on days 1 and 3, with fresh medium replaced on the day of observation (Supplementary Figs. S14 and S17). However, activation was still detectable with no significant change on day 3 (Supplementary Fig. S17).

Next, we investigated PPSU-4Ad for its ability to induce antigen-specific T cell proliferation in vivo using the OT-1 mouse strain (Fig. 5a). This strain has a transgenic T cell receptor designed to recognize OVA, resulting in MHC class I-restricted, OVA-specific, $CD8^+$ T cell proliferation upon successful vaccination against OVA as an antigen[35]. C57BL/6 mice were immunized with PPSU-4Ad, single adjuvant (PPSU-CpG or PPSU-MPLA) or only antigen (PPSU-OVA) loaded hydrogels subcutaneously at the tail base. Then, $CD8^+$ T cells isolated from OT-1 transgenic mice were stained with Carboxyfluorescein succinimidyl ester (CFSE) dye and adoptively transferred to mice one day post immunization. 96 h later, the mice were sacrificed, inguinal lymph nodes (LNs) and spleen were harvested. First, we tested the activation marker expression on $CD11C^+$ DCs in the LNs. Consistent with the in vitro results, PPSU-4Ad significantly upregulated MHC-II, CD40, CD80, and CD86 expression on $CD11c^+$ DCs in the LNs (Fig. 5d, e). Moreover, significant proliferation of $CFSE^+$ OT-1 $CD8^+$ T cells in both

https://doi.org/10.1038/s41467-025-60416-x

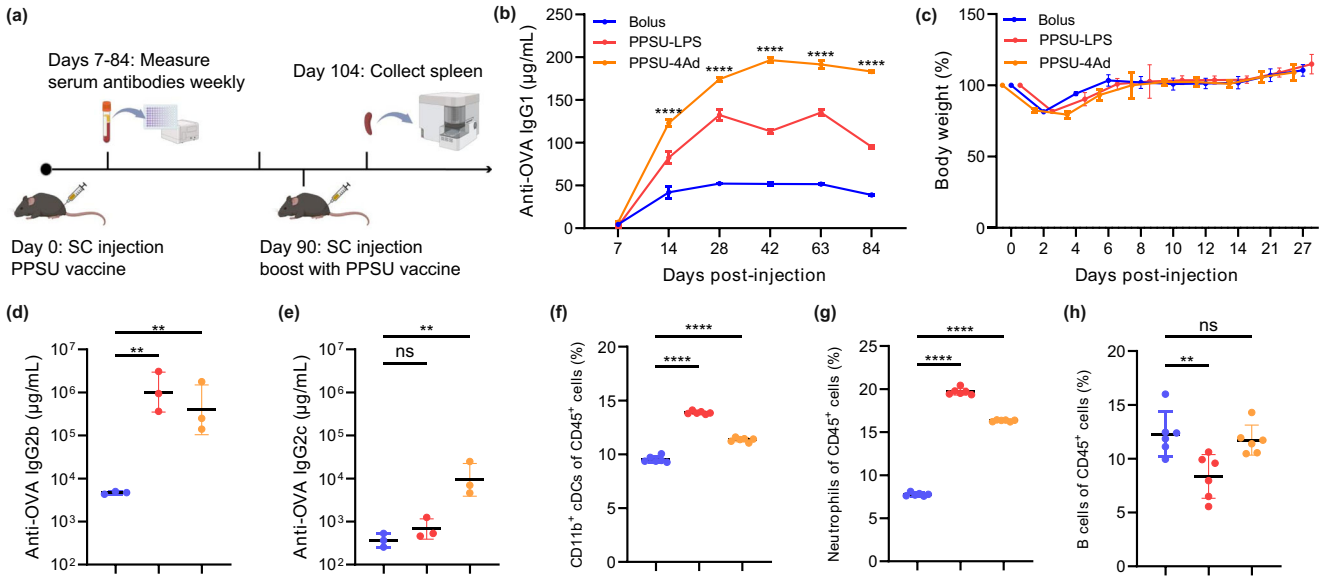

Fig. 6 | Long-term presentation of subunit PPSU vaccines after a single administration. a Experimental timeline: Antibody concentrations were measured after a single subcutaneous injection of either a bolus formulation (100 μg OVA, 20 μg CpG, 25 μg MPLA, 25 μg CL429, and 25 μg LPS) or PPSU vaccines containing one (PPSU-LPS) or four adjuvants (PPSU-4Ad). Measurements began on day 7 and continued until day 84. **b** Serum anti-OVA IgG1 concentrations: ($n = 6$ animals per group; samples pooled and measured in triplicate). Data are presented as mean ± S.D., with **** $p < 0.0001$ compared to bolus and PPSU1, determined using two-way ANOVA followed by Sidak's multiple comparison test. **c** Mouse body weight changes: Weight changes were monitored after vaccination ($n = 6$ animals per group). Data are presented as mean ± S.D. **d**, **e** Serum anti-OVA IgG2b and IgG2c concentrations: These were evaluated on day 28 post-vaccination ($n = 6$ animals per group; samples pooled and measured in triplicate). Data are presented as mean ± S.D. ns: no significant difference compared to bolus; ** p (0.0013, 0.0036, IgG2b), p (0.0019, IgG2c) < 0.01 compared to bolus, determined using one-way ANOVA followed by Tukey's multiple comparison test. **f**–**h** Flow cytometry analysis of CD45$^+$ splenic cell populations 2 weeks post-boost ($n = 6$ animals per group; data presented as mean ± S.D). ns no significant difference compared to bolus; ** p (0.0058, B cells) <0.01 compared to bolus, **** $p < 0.0001$ compared to bolus, determined using one-way ANOVA followed by Tukey's multiple comparison test: **f** CD11b$^+$ conventional dendritic cells (cDCs), **g** Neutrophils, and **h** B cells.

LNs and spleen was observed in mice immunized with PPSU-4Ad, compared to PPSU groups loaded with only a single adjuvant or antigen (Fig. 5f, g). Without additional adjuvants, the single adjuvant and PPSU-OVA groups showed a limited number of divisions in vivo at 4 days post-transfer, similar to the findings reported previously[36,37]. To determine whether a single administration of PPSU-4Ad could provide sustained vaccine exposure and thereby augment both the magnitude and duration of the humoral response, we conducted an ~90-day ovalbumin vaccination study (Fig. 6a). Notably, the peak levels of OVA-specific serum IgG1 were 4 times higher in mice receiving the sustained-release PPSU-4Ad formulation compared to the bolus formulation and 2 times higher compared to PPSU-LPS, which contains a single adjuvant loaded with a high dose of LPS (Fig. 6b). Body weight in all groups returned to their original levels within 10 days post-injection (Fig. 6c). PPSU-4Ad exhibited significantly higher IgG2b and IgG2c levels compared to the bolus formulation, even 28 days after a single administration (Fig. 6d, e), while IgG1 levels were maintained for up to 84 days (Fig. 6b). Although PPSU-4Ad increased IgG2b and IgG2c concentration relative to the bolus, the overall IgG2/IgG1 ratio was lower due to a more pronounced IgG1 response, suggesting a predominantly Th2-skewed humoral profile. The concentrations of IgG1, IgG2b, and IgG2c align with previous reports in ovalbumin-immunized C57BL/6 mice[38–40], and the concurrent elevation of IgG2 subclasses indicates that the sustained-release depot also engaged Th1-associated pathways, contributing to a broader and more potent antibody response than the bolus control. Moreover, early serum cytokine profiling (Fig. 5b) revealed that at 24 h post-injection, PPSU-4Ad induced both Th1 and Th2 serum cytokines, with notably elevated Th2 levels further supporting its robust humoral immunogenicity. To study the prime-boost response, we administered the same initial dose 90 days after the first vaccination and assessed the response 15 days post-boost (Fig. 6a). The spleen was selected as the primary site for immune analysis because it integrates circulating immune responses from sustained antigen and adjuvant release[41,42] and, owing to its abundant immune cell populations, provides a robust readout of long-term systemic immunity[43]. Following 14 days after a booster administered at 90 days post-initial vaccination, mice receiving the sustained-release PPSU-4Ad formulation exhibited significantly elevated frequencies of CD11b$^+$ cDCs and neutrophils in the spleen, while B cell levels remained similar to those observed with bolus control (Fig. 6f, h and Supplementary Fig. S18). These data suggest that the PPSU-4Ad maintains an immunological environment resembling the early stages of vaccination, effectively prolonging antigen and adjuvant availability[3]. Despite normalization of total B cell frequencies, the prolonged presence of activated myeloid cells likely reflects ongoing antigen and adjuvant availability, which helps preserve memory B cell and plasma cell function over time. Consistent with this idea, the sustained activation of innate myeloid cells can actively support long-term humoral immunity – for example, persistent CD11b$^+$ cDCs and neutrophils have been linked to enhanced antibody responses, in part by providing prolonged antigen presentation and survival signals that maintain plasma cells[44,45]. Moreover, durable antigen-specific IgG can be maintained even without bulk B cell expansion, as long-lived plasma cells residing in survival niches continue to secrete antibody for extended periods in the absence of ongoing B cell proliferation or reactivation[46,47]. Collectively, these results verify that PPSU-based hierarchical hydrogels effectively co-deliver antigen and multiple physicochemically distinct adjuvants for synergistic immune responses following subcutaneous administration. Additionally, fine-tuning the antigen-specific immune responses is straightforward due to the capacity for ratiometric loading, achievable by varying the combinations of antigen and adjuvants.

Our studies demonstrate a hierarchical hydrogel-based platform for the engineering of synthetic subunit vaccines with biomimetic,

synergistic immune responses. The strategy involves ratiometric loading and tissue attachment that make use of a self-assembling homopolymer, which assembles into nanogels in water, then to microgels in saline, and ultimately to tertiary hydrogels in vivo. When delivering four physicochemically distinct adjuvants and a protein antigen, the hydrogels elicited vaccine-related immune responses both in vitro and in vivo that were superior to standard bolus and single adjuvant formulations. These minimalist hierarchical hydrogels, formed from a single simple homopolymer, achieve efficient ratiometric loading to simplify complex drug delivery applications where controlling multiple drug concentrations is tedious or not feasible.

Methods

Chemicals and reagents

All chemicals were purchased from Sigma-Aldrich and used as received, unless otherwise stated. HBB (lyophilized powder) was obtained from Sigma (H2500; LOT# SLCB6082). Ethylenediaminetetraacetic acid disodium salt solution, albumin from chicken egg white, and corning® transwell® 24 well plates were purchased from Sigma-Aldrich (St. Louis, MO, USA). Invitrogen™ eBioscience™ 1X RBC Lysis Buffer, Falcon™ Cell Strainers, Falcon™ Round-Bottom Polystyrene Test Tubes with Cell Strainer Snap Cap 5 mL, Propylene Sulfide (stabilized with Butyl Mercaptan) 98.0+%, Heat-Inactivated Fetal Bovine Serum (FBS), Gibco Dulbecco's Modified Eagle's medium (DMEM), Gibco Roswell Park Memorial Institute 1640 medium (RPMI), Gibco Dulbecco's Phosphate Buffered Saline (without calcium chloride and magnesium chloride), hexamethyldisilazane (HMDS), Th1/Th2 cytokine ELISA kit (Invitrogen), Hyaluronidase Type I-S from Bovine, Ethanol (200 Proof), Indocyanine Green, carboxyfluorescein succinimidyl ester (CFSE), Percp-eFlour710 anti-mouse CD80, BV480 anti-mouse CD3, and Methotrexate Fluorescein Triammonium Salt were purchased from Thermo Fisher Scientific (Waltham, MA, USA). Lipopolysaccharide (LPS), CL429, CpG oligodeoxynucleotide, Class C (CpG-ODN), monophosphoryl lipid A (MPLA),and QUANTI-Blue substrate were purchased from InvivoGen (San Diego, CA, USA). Collagenase, Type 4 and Deoxyribonuclease I were purchased from Worthington Biochemical (Lakewood, New Jersey, USA). Mouse Anti-OVA IgM Antibody Assay Kit was purchased from Chondrex, Inc (Woodinville, WA, USA). Flow cytometry cell staining buffer (1 ×), anti-mouse CD16/CD32, fixable zombie NIR viability dye and all antibody cocktail (PE-Cy5 anti-mouse MHC-II, PE-Cy7 anti-mouse CD40, APC anti-mouse CD80, APC-Cy7 anti-mouse CD11c, PerCP-Cy5.5 anti-mouse CD45, BV510 anti-mouse CD3 and PE-Dazzle594 anti-mouse CD86, PE-Fire 700 anti-mouse CD11c, BV421 anti-mouse CD11b, PE-Dazzle 594 anti-mouse F4/80, BV605 anti-mouse Ly-6C, BV650 anti-mouse MHC II (I-A/I-E), FITC anti-mouse Ly6G, BV785 anti-mouse NK1.1, PerCP anti-mouse CD19, BV480 anti-mouse CD3, and BV570 anti-mouse CD45) were purchased from BioLegend (San Diego, CA, USA). BUV563 anti-mouse CD8a was purchased from BD Biosciences (Franklin Lakes, NJ, USA). BD Veo U-100 Syringes 31 g 3/10cc 6 mm 90 Count was purchased from ADW Diabetes (Pompano Beach, FL, USA). STEMCELL $CD8a^+$ T Cell Isolation Kit was purchased from STEMCELL Technologies (Vancouver, BC, Canada). InVivoMAb anti-mouse TNF-α and InVivoPure pH 7.0 Dilution Buffer were purchased from Bio X Cell (Lebanon, NH, USA). Mouse Anti-Ovalbumin antibody assay kits for IgG2b, IgG2c were purchased from Chondrex, Inc (Woodinville, WA, USA). Mouse Anti-Ovalbumin IgG1 ELISA Kit was purchased from Cayman Chemical Company (Ann Arbor, Michigan, USA).

Preparation of PPSU

$PPSU_{20}$ was synthesized in our previous paper[12]. First, poly(propylene sulfide) (PPS) was prepared by anionic ring-opening polymerization of propylene sulfide (20 equiv.) using ethanethiol (1 equiv.) initiator and benzyl bromide (5 equiv.) end-capper in the presence of sodium methylate as a base in dry dimethyl formamide. The PPS homopolymers were collected and purified by precipitation in methanol three times. Then, mixing PPS with 30% of hydrogen peroxide (1 g PPS per 20 mL of 30% of hydrogen peroxide) and shaking the mixtures led to a homogeneous solution overnight. Lyophilization of the obtained solution resulted in shiny solids of PPSU without the requirement for further purification. ^{1}H NMR (500 MHz, DMSO-d6, δ, ppm) 7.5-7.3 (m, 5H), 4.7-4.6 (s, 2H), 4.2-3.7 (m, 40H), 3.7-3.2 (m, 20H), 1.6-1.4 (m, 60H).

Labeling PPSU with perylene bisimide (PBI)

Amine functionalized poly(propylene sulfide) (PPS_{42}-NH_2) was synthesized by anionic ring opening polymerization and bridged via PBI to form PPS-PBI-PPS, following the protocol described in our previous paper[48]. First, PPS-NH_2 was prepared by the anionic ring-opening polymerization of propylene sulfide (40 equiv.) using 2-aminoethanethiol (1 equiv.) initiator and acetic acid (5 equiv.) end-capper in the presence of sodium methylate as a base in dry dimethyl formamide. The polymers (PPS-NH_2) were collected and purified by precipitation in methanol three times. Second, PBI-bridged polymers (PPS-PBI-PPS) were synthesized by reaction of perylene-3,4,9,10-tetracarboxylic dianhydride (PTCDA) with PPS-NH_2. PTCDA (1 equiv.) and PPS-NH_2 (2 equiv.) were mixed in pyridine, then heated with stirring at 150 °C for 2 days. As the mixture cooled, the mixture was diluted in tetrahydrofuran, followed by filtration. The filtrate was concentrated and precipitated in methanol three times to yield the product of PPS-PBI-PPS. Third, mixing the PPS-PBI-PPS with 30% of hydrogen peroxide (1 g polymer per 20 mL of 30% of hydrogen peroxide) and shaking the mixtures led to a homogeneous solution overnight. Lyophilization of the obtained red solution resulted in red solids of PPSU-PBI-PPSU without the requirement for further purification. ^{1}H NMR (500 MHz, DMSO-d6, δ, ppm) 8.8-8.3 (m, 4H), 7.2-6.5 (m, 4H), 4.1-3.6 (m, 84H), 3.6-3.1 (m, 42H), 1.6-1.3 (m, 126H).

Preparation of PPSU hydrogels

200 µL of PPSU in DMSO (25 mg/mL; with or without co-dissolved cargoes) were thoroughly mixed with 200 µL of water. The obtained 400 µL of mixtures were further thoroughly mixed with 200 µL of water. Dialysis in water (Slide-A-Lyzer Dialysis Cassettes, 10 K MWCO) was then performed to completely remove DMSO. The obtained PPSU nanogels were stocked at 4 °C for further use. PPSU microgels were prepared by mixing 900 µL of PPSU nanogels (5 mg/mL in water; with or without co-dissolved antigen or adjuvants) with 100 µL of PBS (10×). After 5-min incubation, the mixture was centrifuged (15,000 × g for 5 min), and the microgel pellet was collected by discarding the supernatant. The pellet was resuspended in fresh PBS, followed by repeating the centrifugation-resuspension cycle for a total of three times to remove unbound antigen or adjuvants. The microgels were resuspended in PBS (10 mg/mL) for injection.

Animals

All procedures involving animals received approval from Northwestern University's Institutional Animal Care and Use Committee, adhering to the NIH guidelines for the ethical treatment and utilization of laboratory animals. All in vivo studies were conducted exclusively in female mice. To avoid introducing additional variables over long-term vaccination studies, we exclusively used female mice, ensuring that observed differences in treatment outcomes reflected the interventions rather than sex-based variability. Female BALB/c mice, C57BL/6 mice, and C57BL/6-Tg(TcraTcrb)1100Mjb/J (OT-1, JAX stock #003831) mice, all aged 6–8 weeks, were procured from the Jackson Laboratory in Bar Harbor, Maine, USA. Animals were housed in Northwestern University's Center for Comparative Medicine under controlled conditions (18–23 °C, 40–60% relative humidity) on a 12 h light/12 h dark cycle. All injections were administered using BD Veo U-100 syringes (31 G, 3/10 cc, 6 mm).

Fluorescence measurement
Fluorescence spectra were recorded by an RF-6000 spectrofluorometer using LabSolutions RF software.

TEM imaging
Negative staining was used for imaging the samples. To prepare the staining reagent, 1.5% uranyl formate (UF) was dissolved in water. The pH was then adjusted to 4.5 by the addition of 10 M KOH. Formvar carbon film grids (FCF400-CU; Electron Microscopy Sciences) were treated for 20 s in a Pelco easiGlow glow discharger (0.24 mbar; 15 mA). A pretreated grid was suspended upside down in 20 µL of hydrogel suspension (0.7 mg/mL) for 30 s. The sample-loaded grid was further suspended upside down in 30 µL of 1.5% UF twice for 15 s, followed by the removal of excess UF solution by blotting with Whatman filter paper. TEM Images were acquired at 30 k on a JOEL 1400 TEM operating at 120 kV and processed in ImageJ (v.1.53e) software.

Cryo-TEM imaging
Fresh samples were prepared by applying 3 µL of suspension on pretreated (same as TEM imaging) holey lacey carbon 400 mesh TEM copper grids (Electron Microscopy Sciences). Following a blot of 3 s, the grids were plunge-frozen (Gatan Cryoplunge 3 freezer). Images were acquired using a field emission transmission electron microscope (JEOL 3200FS) operating at 300 keV. Digital Micrograph software (Gatan) was used to align the individual frames of each micrograph to compensate for stage and beaminduced drift. Any further image processing was completed in ImageJ (v.1.53e) software.

Cryo-SEM imaging
300-mesh Cu grids with a carbon membrane were glow-discharged for 30 s in a Pelco easiGlow glow-discharger at 15 mA with a chamber pressure of 0.24 mBar. 5 µL of samples were pipetted onto a grid and briefly blotted by hand while paying careful attention to make sure the liquid layer did not dry before plunging the grid into liquid ethane. Grids were then loaded into a Gatan 626.5 cryo transfer holder and viewed in a Hitachi HD2300 STEM with a field emission source at 200 kV utilizing an SE detector. Prior to gathering image data, the cryo transfer holder was warmed from −180 °C to −145 °C at a rate of 5 °C/min. This warming process slowly sublimed away background ice under vacuum to reveal particles. The image data were collected with a Gatan digital micrograph and a DigiScan system and processed in ImageJ (v.1.53e) software.

All atom explicit solvent molecular dynamics simulations
The 125-chain PPSU nanoparticle was obtained by the previous simulations[17]. Indocyanines (ICG) molecule was built with the package Avogadro[49]. The CHARMM force field parameter for ICG was generated with CGenFF[50]. After the simulation of 125-chain nanoparticle approached equilibrium, 10 molecules of ICG were solvated into the system along with the counter-ions (10 Na^+). The ICG molecules were distributed randomly in the simulation box. Energy minimization, NVT equilibration, NPT equilibration, and 200 ns molecular dynamics production run were performed with the same simulation parameters aforementioned. The binding energy between ICGs and the nanoparticle was calculated with the *gmx energy* tool.

Loading efficiency
2,3-cGAMP (Invivogen) was quantified by liquid chromatography-mass spectrometry (C18 column) using linear gradient eluents of 0–98% B mixed with A from 1 to 3 min (A: 0.1% formic acid; B: acetonitrile with 0.1% formic acid) at 0.6 mL/min at 50 °C.CL429 (Invivogen) was quantified by a colorimetric assay that forms metal-complex with the absorbance at 660 nm. The loading efficiencies of Alexa-647-labeled OVA (Invivogen; $\lambda_{em}/\lambda_{ex}$ = 668/650 nm), FITC-labeled CpG-ODN (Invivogen; $\lambda_{em}/\lambda_{ex}$ = 525/495 nm), and cy3-labeled LPS (Nanocs; $\lambda_{em}/\lambda_{ex}$ = 570/550 nm) were determined by fluorescence measurements.

Rheological characterization
200 µL of hydrogels (10 mg/mL in PBS) was subcutaneously administered to the C57BL/6 female mouse neck. After 30 min, the injection site was excised, and the hydrogel was retrieved from the skin. Rheological analysis was conducted at 37 °C in a humidified atmosphere using modular compact rheometer (Anton Paar MCR302). All measurements were performed using an 8 mm parallel plate geometry with a 0.3 mm gap height. An amplitude sweep was performed at a constant angular frequency of 6.28 rad s^{-1} to verify the linear viscoelastic regime. Frequency dependence of the storage and loss moduli was analyzed in oscillatory mode in the linear viscoelastic regime (0.1%).

SEM-EDS analysis
The nanogels were loaded with 5 wt.% of deferoxamine mesylate (DFOM). Excess $FeCl_3$ was added to induce microgel formation and coordination. The hydrogels were centrifuged, and the pellet was collected. The pellet was resuspended in PBS, followed by centrifugation. This step was repeated a total of three times to prepare $FeCl_3$-loaded hydrogels. Before injection, the C57BL/6 female mouse neck area was shaved, and remaining hair was removed using Nair. A subcutaneous injection of 200 µL of the $FeCl_3$-loaded hydrogels (10 mg/mL in PBS) was administered to the neck. After 30 min, the skin along with hydrogels was collected for SEM analysis. A 2.5% glutaraldehyde solution was applied for fixation for two hours at room temperature (glutaraldehyde was diluted from 25% with 0.1 M sodium cacodylate buffer, which was further diluted from 0.4 M sodium cacodylate buffer with water). The skins with hydrogels were then rinsed three times with 0.1 M sodium cacodylate buffer and once with water (each rinse lasting 10 min) and incubated in 2% osmium tetroxide for 30 min. After another three rinses with water (each lasting 10 min), the sample underwent dehydration with a series of ethanol gradients (30%, 50%, 70%, 85%, and 95%) for 10 min at each step. The dehydrated cells were rinsed with 100% ethanol two times for 10 min each and were immersed in 1:1 mixture of HMDS and ethanol for 30 min and were subsequently rinsed twice with 100% HMDS for 30 min each. After overnight drying, the cells were placed on a carbon tape attached to an aluminum stud and coated with SPF Osmium Coater (21 nm thickness) for SEM-EDS analysis. The morphology and Fe content were then observed using a Hitachi SU-8030 C-FEG SEM and Oxford Instrument X-Max 80 energy dispersive x-ray spectroscopy (EDS) detector. Due to the electron beam sensitive of the sample, a beam energy of 15 kV was used for x-ray microanalysis to see the Fe Kα peak at 6.4 eV. EDS spectral maps were collected for several areas of interest to determine the spatial distribution of elements. Areas concentrated in Fe were then probed individually to determine the presence and relative wt.% Fe in those areas (AZtec version 6.1).

In vivo release
Either 20 µg of ICG ($\lambda_{em}/\lambda_{ex}$ = 800/745 nm) or 20 µg of ICG adsorbed by 2 mg of hydrogels in 200 µL was subcutaneously administered to the neck of Female BALB/c mice. Live monitoring of ICG was conducted at different time points: 0, 1, 2, 3, and 5 days. For FRET analysis, 0.5 wt.% of Rh6G were encapsulated in PPSU nanogels, followed by the adsorption of 0.5 wt.% of Rh101. 200 µL of the resulting hydrogel suspension in PBS (10 mg/mL of PPSU) was subcutaneously administered to the neck of Female BALB/c mice. The mouse was euthanized at various time points, including 0.5 h, 1, 3, 5, 7, 10, 14, and 21 days. The skins containing hydrogels were excised and imaged using IVIS Lumina ($\lambda_{em}/\lambda_{ex}$ = 465/640 nm for Rh101, $\lambda_{em}/\lambda_{ex}$ = 465/560 nm for Rh6G). Similarly, 2 wt.% of fluorescein-labeled methotrexate (MFT) were encapsulated in PPSU nanogels, followed by the adsorption of excess TNF-α (labeled with tetramethylrhodamine isothiocyanate) in PBS. The unbound TNF-α was removed. 200 µL of the resulting hydrogel suspension in PBS (10 mg/mL of PPSU) was subcutaneously administered to the neck of Female BALB/c mice. The mouse was euthanized, then

the skin was excised at various time points, including 0.5 h, 1, 3, 7, 14, 21, 28, 42, 56, and 92 days for IVIS analysis. Images were then analyzed using IVIS Lumina ($\lambda_{em}/\lambda_{ex}$ = 465/600 nm for TNF-α, $\lambda_{em}/\lambda_{ex}$ = 465/520 nm for MFT). The v.4.5.5, PerkinElmer Image Software was used for IVIS.

In vitro adjuvant activity assay

NF-kB/AP-1 activation was assessed in RAW-blue macrophages (Invivogen) following the manufacturer's protocols. Cells were washed twice with PBS before use. RAW-blue cells (180 µL) in media (DMEM supplemented with 10% heat-inactivated FBS and 1% Pen/strep) were seeded at a density of 10^5 cells/well in 96-well plates. Samples with varying concentrations in a PBS solution (20 µL) were added to each well. After 24 h, 50 µL of culture supernatants were collected and incubated with 150 µL of QUANTI-Blue substrate (Invivogen) for 2 h. The level of secreted embryonic alkaline phosphatase (SEAP) was determined using an M3 plate reader (SpectraMax) at an absorbance of 655 nm (Softmax Pro 6 version 6.3).

In vivo blood analysis

C57BL/6 mice were subcutaneously immunized with either 100 µL of OVA-CpG PPSU or OVA-CpG-MPL-CL429 mult-adjuvant PPSU. Controls included mice injected with blank PPSU and PBS only. Each mouse received a dosage of 30 µg of OVA, 20 µg of CpG, 25 µg of MPL, and 25 µg of CL429. At 24 h post-injection, blood samples were collected, and serum cytokines were quantified using a Th1/Th2 cytokine ELISA kit. Seven days post-immunization, all mice were euthanized, and whole blood was obtained for the analysis of serum anti-OVA IgM antibodies using a Mouse Anti-OVA IgM Antibody Assay Kit (an M3 plate reader (SpectraMax) and Softmax Pro 6 version 6.3).

Mouse primary bone-marrow-derived dendritic cells (BMDCs)

Bone marrow cells were harvested from the isolated tibias and femurs of C57BL/6 mice. The procedure involved removing muscles and connective tissues from the bone, followed by flushing the cut ends of the bones using a syringe filled with complete RPMI-1640 medium (supplemented with 10% heat-inactivated FBS and 1% Pen/strep). The bone marrow suspensions were transferred into a sterile 15 mL centrifuge tube and centrifuged at 400 × *g* for 5 min. Subsequently, the suspended cells were resuspended in complete RPMI-1640 medium supplemented with GM-CSF (20 ng/mL). The cells were plated at a density of 2×10^6 cells per well in 6-well plates and incubated at 37 °C in a 5% CO2 humidified incubator for 6 days. Half of the medium was replaced with fresh GM-CSF-containing medium on day 3. After 6 days, non-adherent and loosely adherent cells were treated with 100 µg of PPSU that contained 100 ng of MPLA, 100 ng of CL429, 100 ng of LPS, 100 ng of CPG-ODN, 10 µg of OVA and incubated for an additional 24 h for flow cytometry analysis. The following cocktail was used: PE-Cy5 anti mouse MHC-II (BioLegend; clone M5/114.15.2; Cat #: 107612; Lot #: B383697; 1:400), PE-Cy7 anti mouse CD40 (BioLegend; clone 3/23; Cat #: 124622; Lot #: B239100; 1:100), APC anti mouse CD80 (BioLegend; clone 16-10A1; Cat #: 104713; Lot #: B271483; 1:100), PE-Dazzle594 anti mouse CD86 (BioLegend; clone GL-1; Cat #: 105042; Lot #: B353566; 1:400). All PPSU Groups contained OVA protein (1 wt.% of PPSU). The mean fluorescence intensity (MFI) was quantified by flow cytometry using a 3 L 16V-14B-8R Aurora flow cytometer (CyTek). Spectral unmixing (SpectroFlo version 3.2.1) was completed using SpectroFlo (CyTek), followed by the analysis using FlowJo software (v10.10.0).

In vitro evaluation of adjuvant activity for in situ formed hydrogels

C57BL/6 mice were immunized with the same dose of PPSU-4Ad used for BMDCs. PPSU-LPS contained the same dose of ovalbumin but included only a single adjuvant, 500 ng of LPS. The gels were retrieved 30 min post-injection and placed on the transwell insert. The in vitro adjuvant activity assay protocol, described above, was then used to evaluate activity at days 1 and 3, with fresh medium added on the day of measurement.

OT-1 $CD8^+$ adoptive T cell in vivo proliferation

C57BL/6 mice were immunized with the same dose as the one administered to BMDCs. $CD8^+$ OT-1 T cells were isolated from the spleens of C57BL/6-Tg(TcraTcrb)1100Mjb/J mice using the STEMCELL $CD8a^+$ T Cell Isolation Kit (STEMCELL Technologies), following the manufacturer's instructions. Purified OT-1 T cells were labeled with a cell proliferation dye, carboxyfluorescein succinimidyl ester (CFSE, Thermo Fisher Scientific), according to the manufacturer's recommended protocol. After labeling, the cells were washed and resuspended in sterile PBS. Labeled OT-1 T cells (1×10^6 cells in 100 µL of PBS) were intravenously injected into recipient OT-1 mice via the tail vein. After 96 h, mice were euthanized, and spleens and lymph nodes were harvested for further flow cytometry analysis (same procedure as prior BMDCs experiments and the following cocktail was used PE-Cy5 anti mouse MHC-II (BioLegend; clone M5/114.15.2; Cat #: 107612; Lot #: B383697; 1:400), PE-Cy7 anti mouse CD40 (BioLegend; clone 3/23; Cat #: 124622; Lot #: B239100; 1:100), PerCP-eFlour710 anti mouse CD80 (Invitrogen; clone 16-10A1; Cat #: 46-0801-82; Lot #: 1990193; 1:160), PE-Dazzle594 anti mouse CD86 (BioLegend; clone GL-1; Cat #: 105042; Lot #: B353566; 1:400).

Ovalbumin vaccination

Male C57BL/6 mice were immunized with a single subcutaneous injection of either a bolus formulation (100 µg OVA, 20 µg CpG, 25 µg MPLA, 25 µg CL429, and 25 µg LPS) or one of the PPSU vaccine formulations. PPSU-1 included 100 µg OVA and 100 µg LPS, while PPSU-4 contained the same components as the bolus formulation. Body weight was also monitored throughout the study until it returned to the original weight. Blood samples were collected retro-orbitally at 7, 14, 28, 42, 63, and 84 days post-vaccination and centrifuged at 1.3 G for 10 min to obtain serum. Anti-ovalbumin IgG1, IgG2b, and IgG2c antibody titers were then quantified by ELISA, M3 plate reader (SpectraMax) and Softmax Pro 6 version 6.3, following the manufacturer's instructions.

Flow cytometric analysis

A booster dose, identical to the initial vaccination, was administered 90 days post-vaccination. Two weeks later, spleens were harvested, minced, and passed through a 70-µm filter, followed by centrifugation at 500 g for 5 min. Splenocytes from six mice per group (n = 6 spleens per group) were pooled together. The pellet was treated with red blood cell lysis buffer for 5 min; the lysis reaction was stopped with 1× PBS, and cells were centrifuged at 500 g for 5 min. Single-cell suspensions were incubated with Zombie Near-Infrared viability dye for 15 min and subsequently washed twice. To block Fc receptors, cells were incubated with anti-mouse CD16/CD32 (BioLegend; clone 93; Cat #: 101302; Lot #: B341164; 1:100) for 15 min. Cells were then stained for 30 min with a cocktail of fluorophore-conjugated antibodies, including PE-Fire 700 anti-mouse CD11c (BioLegend; clone QA18A72; Cat #: 161108; Lot #: B379902; 1:200), BV421 anti-mouse CD11b (BioLegend; clone M1/70; Cat #: 101236; Lot #: B360997; 1:400), PE-Dazzle 594 anti-mouse F4/80 (BioLegend; clone BM8; Cat #: 123146; Lot #: B375239; 1:200), BV605 anti-mouse Ly-6C (BioLegend; clone HK1.4; Cat #: 128036; Lot #: B335981; 1:20), BV650 anti-mouse MHC II (I-A/I-E) (BioLegend; clone M5/114.15.2; Cat #: 107641; Lot #: B384370; 1:400), FITC anti-mouse Ly6G (BioLegend; clone 1A8; Cat #: 127606; Lot #: B363942; 1:400), BV785 anti-mouse NK1.1 (BioLegend; clone PK136; Cat #: 108749; Lot #: B368822; 1:800), PerCP anti-mouse CD19 (BioLegend; clone 6D5; Cat #: 115532; Lot #: B378614; 1:400), BUV563 anti-mouse CD8a (BD Biosciences; clone 53-6.7; Cat #: 569185; Lot #: 3172693; 1:100), BV480 anti-mouse CD3 (Invitrogen; clone 17A2; Cat #:

414-0032-82; Lot #: 2746378; 1:100), and BV570 anti-mouse CD45 (BioLegend; clone 30-F11; Cat #: 103135; Lot #: B378404; 1:200). Antibodies were diluted according to the manufacturers' recommendations. Finally, cells were washed twice with cell staining buffer and resuspended in the same buffer. Data acquisition was performed using a 3 L 16V-14B-8R Aurora flow cytometer (Cytek). Single-color staining controls and fluorescence-minus-one (FMO) controls were utilized to gate specific cellular populations. A minimum of 100,000 single, live-cell events were recorded. SpectroFlo (Cytek) software (SpectroFlo version 3.2.1) was used for spectral unmixing, and FlowJo software (v10.10.0) was employed for analysis.

Statistical analysis

Statistical analysis of all data was carried out using GraphPad Prism 10.1.2 (La Jolla, CA). Statistical significance was performed by unpaired *t*-test or one/two-way ANOVA followed by the recommended multiple comparisons test. A p-value of <0.05 was considered statistically significant.

Reporting summary

Further information on research design is available in the Nature Portfolio Reporting Summary linked to this article.

Data availability

All data underlying this study are available from the corresponding author upon request.

References

1. Reed, S. G., Orr, M. T. & Fox, C. B. Key roles of adjuvants in modern vaccines. *Nat. Med.* **19**, 1597–1608 (2013).
2. Walvekar, P., Kumar, P. & Choonara, Y. E. Long-acting vaccine delivery systems. *Adv. Drug Deliv. Rev.* **198**, 114897 (2023).
3. Roth, G. A. et al. Designing spatial and temporal control of vaccine responses. *Nat. Rev. Mater.* **7**, 174–195 (2022).
4. Vivier, E. & Malissen, B. Innate and adaptive immunity: specificities and signaling hierarchies revisited. *Nat. Immunol.* **6**, 17–21 (2005).
5. Ou, B. S., Saouaf, O. M., Baillet, J. & Appel, E. A. Sustained delivery approaches to improving adaptive immune responses. *Adv. Drug Deliv. Rev.* **187**, 114401 (2022).
6. Li, J. & Mooney, D. J. Designing hydrogels for controlled drug delivery. *Nat. Rev. Mater.* **1**, 16071 (2016).
7. Eloy, J. O. et al. Liposomes as carriers of hydrophilic small molecule drugs: strategies to enhance encapsulation and delivery. *Colloids Surf. B Biointerfaces* **123**, 345–363 (2014).
8. Fan, Y. et al. Nanogel encapsulated hydrogels as advanced wound dressings for the controlled delivery of antibiotics. *Adv. Funct. Mater.* **31**, 2006453 (2021).
9. Li, S. et al. Antibacterial hydrogels. *Adv. Sci.* **5**, 1700527 (2018).
10. Fang, K. et al. Mechano-responsive, tough, and antibacterial zwitterionic hydrogels with controllable drug release for wound healing applications. *ACS Appl. Mater. Interfaces* **12**, 52307–52318 (2020).
11. Xu, Y. in *Modern inorganic synthetic chemistry*, 2nd ed. (eds Ruren, X. & Yan, X.) 545–574 (Elsevier, 2017).
12. Du, F. et al. Homopolymer self-assembly of poly(propylene sulfone) hydrogels via dynamic noncovalent sulfone–sulfone bonding. *Nat. Commun.* **11**, 4896 (2020).
13. Wang, Y.-Q., Bazin-Lee, H., Evans, J. T., Casella, C. R. & Mitchell, T. C. MPL Adjuvant Contains Competitive Antagonists of Human TLR4. *Frontiers in Immunology* **11**, https://doi.org/10.3389/fimmu.2020.577823 (2020).
14. Pavot, V. et al. Cutting Edge: New Chimeric NOD2/TLR2 Adjuvant Drastically Increases Vaccine Immunogenicity. *J. Immunol.* **193**, 5781–5785 (2014).
15. Knuefermann, P. et al. CpG oligonucleotide activates Toll-like receptor 9 and causes lung inflammation in vivo. *Respiratory Res.* **8**, 72 (2007).
16. Bertani, B. & Ruiz, N. Function and Biogenesis of Lipopolysaccharides. *EcoSal Plus* **8**, https://doi.org/10.1128/ecosalplus.ESP-0001-2018 (2018).
17. Du, F. et al. Controlled adsorption of multiple bioactive proteins enables targeted mast cell nanotherapy. *Nat. Nanotechnol.* https://doi.org/10.1038/s41565-023-01584-z (2024).
18. Burke, J. A. et al. Subcutaneous nanotherapy repurposes the immunosuppressive mechanism of rapamycin to enhance allogeneic islet graft viability. *Nat. Nanotechnol.* **17**, 319–330 (2022).
19. Du, F., Bobbala, S., Yi, S. & Scott, E. A. Sequential intracellular release of water-soluble cargos from Shell-crosslinked polymersomes. *J. Controlled Rel.* **282**, 90–100 (2018).
20. Vincent, M. P. et al. Surface chemistry-mediated modulation of adsorbed albumin folding state specifies nanocarrier clearance by distinct macrophage subsets. *Nat. Commun.* **12**, 648 (2021).
21. Karabin, N. B. et al. Sustained micellar delivery via inducible transitions in nanostructure morphology. *Nat. Commun.* **9**, 624 (2018).
22. Barman, S. et al. Shaping neonatal immunization by tuning the delivery of synergistic adjuvants via nanocarriers. *ACS Chem. Biol.* **17**, 2559–2571 (2022).
23. Dowling, D. J. et al. Toll-like receptor 8 agonist nanoparticles mimic immunomodulating effects of the live BCG vaccine and enhance neonatal innate and adaptive immune responses. *J. Allergy Clin. Immunol.* **140**, 1339–1350 (2017).
24. Shang, S. et al. Induction of mycobacterium tuberculosis lipid-specific T cell responses by pulmonary delivery of mycolic acid-loaded polymeric micellar nanocarriers. *Front. Immunol.* **9**, 2709 (2018).
25. Irvine, D. J., Swartz, M. A. & Szeto, G. L. Engineering synthetic vaccines using cues from natural immunity. *Nat. Mater.* **12**, 978–990 (2013).
26. Krouskop, T. A., Wheeler, T. M., Kallel, F., Garra, B. S. & Hall, T. Elastic moduli of breast and prostate tissues under compression. *Ultrason Imaging* **20**, 260–274 (1998).
27. Zhang, M. et al. Congruence of imaging estimators and mechanical measurements of viscoelastic properties of soft tissues. *Ultrasound Med. Biol.* **33**, 1617–1631 (2007).
28. Algar, W. R., Hildebrandt, N., Vogel, S. S. & Medintz, I. L. FRET as a biomolecular research tool — understanding its potential while avoiding pitfalls. *Nat. Methods* **16**, 815–829 (2019).
29. Santecchia, I. et al. Innate immune memory through TLR2 and NOD2 contributes to the control of Leptospira interrogans infection. *PLOS Pathog.* **15**, e1007811 (2019).
30. Hernandez, A. et al. The role of MyD88- and TRIF-dependent signaling in monophosphoryl lipid A-induced expansion and recruitment of innate immunocytes. *J. Leukoc. Biol.* **100**, 1311–1322 (2016).
31. Kew, V. G., Wills, M. R. & Reeves, M. B. LPS promotes a monocyte phenotype permissive for human cytomegalovirus immediate-early gene expression upon infection but not reactivation from latency. *Sci. Rep.* **7**, 810 (2017).
32. Seth, A., Heo, M. B. & Lim, Y. T. Poly (γ-glutamic acid) based combination of water-insoluble paclitaxel and TLR7 agonist for chemo-immunotherapy. *Biomaterials* **35**, 7992–8001 (2014).
33. Yuk, S. A. et al. Nanocapsules modify membrane interaction of polymyxin B to enable safe systemic therapy of Gram-negative sepsis. *Sci. Adv.* **7**, https://doi.org/10.1126/sciadv.abj1577 (2021).
34. Gale, E. C. et al. Hydrogel-based slow release of a receptor-binding domain subunit vaccine elicits neutralizing antibody responses against SARS-CoV-2. *Adv. Mater.* **33**, e2104362 (2021).
35. Hogquist, K. A. et al. T cell receptor antagonist peptides induce positive selection. *Cell* **76**, 17–27 (1994).
36. van Stipdonk, M. J. B. et al. Dynamic programming of CD8+ T lymphocyte responses. *Nat. Immunol.* **4**, 361–365 (2003).

37. Jæhger, D. E. et al. Enhancing adoptive CD8 T cell therapy by systemic delivery of tumor associated antigens. *Sci. Rep.* **11**, 19794 (2021).
38. Li, Y. et al. TLR2 deficiency promotes IgE and inhibits IgG1 class-switching following ovalbumin sensitization. *Ital. J. Pediatrics* **47**, 162 (2021).
39. Akache, B. et al. Sulfated archaeol glycolipids: comparison with other immunological adjuvants in mice. *PLOS ONE* **13**, e0208067 (2018).
40. Roth, G. A. et al. Injectable hydrogels for sustained codelivery of subunit vaccines enhance humoral immunity. *ACS Cent. Sci.* **6**, 1800–1812 (2020).
41. Kim, J. et al. Injectable, spontaneously assembling, inorganic scaffolds modulate immune cells in vivo and increase vaccine efficacy. *Nat. Biotechnol.* **33**, 64–72 (2015).
42. Zuccarino-Catania, G. V. et al. CD80 and PD-L2 define functionally distinct memory B cell subsets that are independent of antibody isotype. *Nat. Immunol.* **15**, 631–637 (2014).
43. Bronte, V. & Pittet, M. J. The spleen in local and systemic regulation of immunity. *Immunity* **39**, 806–818 (2013).
44. Palgen, J.-L. et al. Innate and secondary humoral responses are improved by increasing the time between MVA vaccine immunizations. *npj Vaccines* **5**, 24 (2020).
45. Huard, B. et al. APRIL secreted by neutrophils binds to heparan sulfate proteoglycans to create plasma cell niches in human mucosa. *J. Clin. Invest.* **118**, 2887–2895 (2008).
46. Hammarlund, E. et al. Plasma cell survival in the absence of B cell memory. *Nat. Commun.* **8**, 1781 (2017).
47. Amanna, I. J., Carlson, N. E. & Slifka, M. K. Duration of humoral immunity to common viral and vaccine antigens. *N. Engl. J. Med.* **357**, 1903–1915 (2007).
48. Du, F., Liu, Y.-G. & Scott, E. A. Immunotheranostic polymersomes modularly assembled from tetrablock and diblock copolymers with oxidation-responsive fluorescence. *Cell. Mol. Bioeng.* **10**, 357–370 (2017).
49. Hanwell, M. D. et al. Avogadro: an advanced semantic chemical editor, visualization, and analysis platform. *J. Cheminformatics* **4**, 17 (2012).
50. Lee, J. et al. CHARMM-GUI input generator for NAMD, GROMACS, AMBER, OpenMM, and CHARMM/OpenMM simulations using the CHARMM36 additive force field. *J. Chem. Theory Comput.* **12**, 405–413 (2016).

Acknowledgements

This work was supported by the National Institute of Biomedical Imaging and Bioengineering (NIH grant no. 1R01EB030629-01A1) (to E.A.S.). The authors express gratitude to Ao Chen for conducting cryo-TEM observations. The authors are grateful to Eric W. Roth for cryo-SEM observation as well as providing SEM suggestions. This work made use of the BioCryo and EPIC-SEM facilities (RRID: SCR_026361) of Northwestern University's NUANCE Center, which has received support from the SHyNE Resource (NSF ECCS-2025633), the IIN, and Northwestern's MRSEC program (NSF DMR-2308691). Imaging work was performed at the Northwestern University Center for Advanced Molecular Imaging generously supported by NCI CCSG P30 CA060553 awarded to the Robert H Lurie Comprehensive Cancer Center.

Author contributions

F.D., S.A.Y., and Y.Q. contributed equally to this work. F.D. started the studies, prepared the materials, validated the characterization, analyzed the data, and wrote the manuscript. S.A.Y. designed and conducted the in vivo experiments and long-term vaccination studies, validated the in vivo characterization, performed SEM, rheology, and flow cytometry experiments, analyzed the data, and wrote the manuscript. Y.Q. designed and carried out the OT-1 $CD8^+$ adoptive T cell and vaccination experiments, analyzed the data, and wrote the manuscript. E.H.A.M. assisted long-term vaccination studies and performed in vitro assays. M.P.V. and S.B. conducted blood analysis and drug loading experiments. T.M.A. performed the SEM-EDX experiments. H.K. conducted the rheological characterization. Y.L. performed the atomistic simulations. H.L. contributed to the flow cytometry experiment. S.Y. performed the RAW-blue macrophages experiment. B.Q. supervised the simulations. E.S. supervised the entire research process and wrote the manuscript. Figures 1, 5a, and 6a were created with BioRender.com.

Competing interests

The authors declare no competing interests.

Additional information

Supplementary information The online version contains supplementary material available at https://doi.org/10.1038/s41467-025-60416-x.

Correspondence and requests for materials should be addressed to Evan A. Scott.

Peer review information *Nature Communications* thanks Eric Appel and the other, anonymous, reviewer(s) for their contribution to the peer review of this work. A peer review file is available.